

# Role of colliding geometry on the N/Z dependence of balance energy

Sakshi Gautam<sup>a</sup>, Aman D. Sood<sup>b</sup> and Rajeev K. Puri<sup>a1</sup>

<sup>a</sup>*Department of Physics, Panjab University, Chandigarh -160 014, India.*

<sup>b</sup>*SUBATECH, Laboratoire de Physique Subatomique et des Technologies Associées, Université de Nantes - IN2P3/CNRS - EMN 4 rue Alfred Kastler, F-44072 Nantes, France.*

We study the role of colliding geometry on the N/Z dependence of balance energy using isospin-dependent quantum molecular dynamics model. Our study reveals that the N/Z dependence of balance energy becomes much steeper for peripheral collisions as compared to the central collisions. We also study the effect of system mass on the impact parameter dependence of N/Z dependence of balance energy. The study shows that lighter systems shows greater sensitivity to colliding geometry towards the N/Z dependence.

---

<sup>1</sup>Email: amandsood@gmail.com

# 1 Introduction

The construction of radioactive ion beams (RIBs) facilities around the world has generated a lot of interest in isospin physics [1–3]. These facilities provide the opportunities to study the nuclear reactions involving nuclei with neutron or proton excess. These studies are helpful in investigating the structure of rare isotopes and the properties of isospin asymmetric nuclear matter. The ultimate goal of isospin physics by heavy-ion collisions of neutron-rich radioactive nuclei is to explore the isospin dependence of in-medium nuclear effective interactions and the equation of state of asymmetric nuclear matter.

During the last few decades there have been significant activities in exploring the isospin effects in collective flow [4–6] and multifragmentation [7, 8]. Various studies have been done in recent past to investigate the isospin effects in collective flow and in its disappearance (at a particular incident energy called balance energy  $E_{bal}$ ) [4–6, 9, 10]. The isospin effects in collective flow have been explained in literature as the competition among various reaction mechanisms, such as nucleon-nucleon collisions, symmetry energy, surface properties and Coulomb force. The relative importance among these reaction mechanisms is not yet clear [4]. To shed light on the relative importance of above mentioned mechanisms, in Ref. [9, 10] Gautam *et al.* have studied the isospin effects in  $E_{bal}$  and its system size dependence throughout the range of colliding geometry. The study pointed towards the dominance of Coulomb potential in isospin effects at all the colliding geometries. Moreover, the study also pointed that the effect of symmetry energy is uniform throughout the mass range and range of colliding geometries. So to look for an observable which could show the sensitivity to symmetry energy, Sood has studied the N/Z dependence of  $E_{bal}$  for isotopic series of Ca [11]. The study shows that the N/Z dependence of  $E_{bal}$  is sensitive to symmetry energy and shows insensitivity towards the isospin dependence of nucleon-nucleon cross section and henceforth the study revealed that the N/Z dependence of symmetry energy can act as a probe of symmetry energy. To see the system size effects on N/Z dependence of  $E_{bal}$ , followed by this, Gautam and Sood carried out the above mentioned study throughout the mass range at semicentral colliding geometry of  $b/b_{max} = 0.2-0.4$  [12]. Their study showed that the sensitivity of N/Z dependence of  $E_{bal}$  is more for lighter systems. In the present paper, we plan to extend the above study to the whole range of colliding geometries. For the present study we use isospin-dependent quantum molecular dynamics (IQMD) model [13, 14].

## 2 The Model

The IQMD model is an extension of the QMD model [14], which treats different charge states of nucleons, deltas and pions explicitly, as inherited from the Vlasov-Uehling-Uhlenbeck (VUU) model [15]. The IQMD model has been used successfully for the analysis of a large number of observables from low to relativistic energies. The isospin degree of freedom enters into the calculations via symmetry potential, cross sections and Coulomb interaction.

In this model, baryons are represented by Gaussian-shaped density distributions

$$f_i(\vec{r}, \vec{p}, t) = \frac{1}{\pi^2 \hbar^2} \exp(-[\vec{r} - \vec{r}_i(t)]^2 \frac{1}{2L}) \times \exp(-[\vec{p} - \vec{p}_i(t)]^2 \frac{2L}{\hbar^2}) \quad (1)$$

Nucleons are initialized in a sphere with radius  $R = 1.12 A^{1/3}$  fm, in accordance with the liquid-drop model. Each nucleon occupies a volume of  $h^3$ , so that phase space is uniformly filled. The initial momenta are randomly chosen between 0 and Fermi momentum ( $\vec{p}_F$ ). The nucleons of the target and projectile interact by two- and three-body Skyrme forces, Yukawa potential and Coulomb interactions. In addition to the use of explicit charge states of all baryons and mesons, a symmetry potential between protons and neutrons corresponding to the Bethe-Weizsacker mass formula has been included. The hadrons propagate using the Hamilton equations of motion:

$$\frac{d\vec{r}_i}{dt} = \frac{d\langle H \rangle}{d\vec{p}_i}; \quad \frac{d\vec{p}_i}{dt} = -\frac{d\langle H \rangle}{d\vec{r}_i} \quad (2)$$

with

$$\begin{aligned} \langle H \rangle &= \langle T \rangle + \langle V \rangle \\ &= \sum_i \frac{p_i^2}{2m_i} + \sum_i \sum_{j>i} \int f_i(\vec{r}, \vec{p}, t) V^{ij}(\vec{r}', \vec{r}) \\ &\quad \times f_j(\vec{r}', \vec{p}', t) d\vec{r} d\vec{r}' d\vec{p} d\vec{p}'. \end{aligned} \quad (3)$$

The baryon potential  $V^{ij}$ , in the above relation, reads as

$$\begin{aligned} V^{ij}(\vec{r}' - \vec{r}) &= V_{Skyrme}^{ij} + V_{Yukawa}^{ij} + V_{Coul}^{ij} + V_{sym}^{ij} \\ &= [t_1 \delta(\vec{r}' - \vec{r}) + t_2 \delta(\vec{r}' - \vec{r}) \rho^{\gamma-1} (\frac{\vec{r}' + \vec{r}}{2})] \\ &\quad + t_3 \frac{\exp(|(\vec{r}' - \vec{r})|/\mu)}{(|(\vec{r}' - \vec{r})|/\mu)} + \frac{Z_i Z_j e^2}{|\vec{r}' - \vec{r}|} \\ &\quad + t_4 \frac{1}{\rho_0} T_{3i} T_{3j} \delta(\vec{r}_i' - \vec{r}_j'). \end{aligned} \quad (4)$$

Here  $t_6 = 4C$  with  $C = 32$  MeV and  $Z_i$  and  $Z_j$  denote the charges of the  $i$ th and  $j$ th baryon, and  $T_{3i}$  and  $T_{3j}$  are their respective  $T_3$  components (i.e.  $1/2$  for protons and  $-1/2$  for neutrons). The parameters  $\mu$  and  $t_1, \dots, t_4$  are adjusted to the real part of the nucleonic optical potential. For the density dependence of the nucleon optical potential, standard Skyrme-type parametrization is employed.

### 3 Results and discussions

We simulate the reactions of Ca+Ca, Ni+Ni, Zr+Zr, Sn+Sn, and Xe+Xe with  $N/Z$  varying from 1.0 to 2.0 in small steps of 0.2. In particular we simulate the reactions of  $^{40}\text{Ca}+^{40}\text{Ca}$ ,  $^{44}\text{Ca}+^{44}\text{Ca}$ ,  $^{48}\text{Ca}+^{48}\text{Ca}$ ,  $^{52}\text{Ca}+^{52}\text{Ca}$ ,  $^{56}\text{Ca}+^{56}\text{Ca}$ , and  $^{60}\text{Ca}+^{60}\text{Ca}$ ;  $^{56}\text{Ni}+^{56}\text{Ni}$ ,  $^{62}\text{Ni}+^{62}\text{Ni}$ ,  $^{68}\text{Ni}+^{68}\text{Ni}$ ,  $^{72}\text{Ni}+^{72}\text{Ni}$ , and  $^{78}\text{Ni}+^{78}\text{Ni}$ ;  $^{81}\text{Zr}+^{81}\text{Zr}$ ,  $^{88}\text{Zr}+^{88}\text{Zr}$ ,  $^{96}\text{Zr}+^{96}\text{Zr}$ ,  $^{104}\text{Zr}+^{104}\text{Zr}$ , and  $^{110}\text{Zr}+^{110}\text{Zr}$ ;  $^{100}\text{Sn}+^{100}\text{Sn}$ ,  $^{112}\text{Sn}+^{112}\text{Sn}$ ,  $^{120}\text{Sn}+^{120}\text{Sn}$ ,  $^{129}\text{Sn}+^{129}\text{Sn}$ , and  $^{140}\text{Sn}+^{140}\text{Sn}$ ; and  $^{110}\text{Xe}+^{110}\text{Xe}$ ,  $^{120}\text{Xe}+^{120}\text{Xe}$ ,  $^{129}\text{Xe}+^{129}\text{Xe}$ ,  $^{140}\text{Xe}+^{140}\text{Xe}$ , and  $^{151}\text{Xe}+^{151}\text{Xe}$  at  $b/b_{max} = 0.2 - 0.4$ ,  $0.4 - 0.6$  and  $0.6 - 0.8$ . We also use a soft equation of state along with the standard isospin- and energy-dependent cross section reduced by 20%, i.e.  $\sigma = 0.8 \sigma_{nn}^{free}$ . The details about the elastic and inelastic cross sections for proton-proton and proton-neutron collisions can be found in [13, 16]. The cross sections for neutron-neutron collisions are assumed to be equal to the proton-proton cross sections. The reactions are followed till the transverse in-plane saturates. In the present study we use the quantity "directed transverse momentum  $\langle p_x^{dir} \rangle$ " which is defined as [17, 18]

$$\langle p_x^{dir} \rangle = \frac{1}{A} \sum_{i=1}^A \text{sign}\{y(i)\} p_x(i), \quad (5)$$

where  $y(i)$  and  $p_x(i)$  are, respectively, the rapidity and the momentum of the  $i^{th}$  particle. The rapidity is defined as

$$Y(i) = \frac{1}{2} \ln \frac{\vec{E}(i) + \vec{p}_z(i)}{\vec{E}(i) - \vec{p}_z(i)}, \quad (6)$$

where  $\vec{E}(i)$  and  $\vec{p}_z(i)$  are, respectively, the energy and longitudinal momentum of the  $i^{th}$  particle. In this definition, all the rapidity bins are taken into account. It is worth mentioning that the  $E_{bal}$  has the same value for all fragments types [5, 19–21]. Further the apparatus corrections and acceptance do not play any role in calculation of the  $E_{bal}$  [19, 21, 22].

In fig. 1 we display the  $N/Z$  dependence of  $E_{bal}$  for  $b/b_{max} = 0.2-0.4$  (top panel),  $0.4-0.6$  (middle panel) and  $0.6-0.8$  (bottom panel). From figure, we find that at all the colliding geometries  $E_{bal}$  follows a linear behaviour with  $N/Z$ . The slopes are 33, 25, 21, 18, and 15 (at  $b/b_{max} = 0.2-0.4$ ), 58, 41, 27, 19, and 18 (at  $b/b_{max} = 0.4-0.6$ ) and 187, 115, 67, 39, and 36 (at  $b/b_{max} = 0.6-0.8$ ) for the series of Ca, Ni, Zr, Xe and Sn, respectively. From figure, we find that

- (i) the  $N/Z$  dependence of  $E_{bal}$  is steeper for the lighter systems as compared to the heavier systems at all the colliding geometries,
- (ii) for a particular isotopic series, the  $N/Z$  dependence of  $E_{bal}$  is more at peripheral colliding geometry.
- (iii) and the change in slope is more for lighter systems as compared to the heavier systems when we move from central to peripheral colliding geometries. From figure, we see that for Ca series, slope increases by almost 400% when we move from central to peripheral collisions, whereas for Xe series increase in slope is almost 150%.

In Ref. [11] Sood has shown that  $N/Z$  dependence of  $E_{bal}$  is sensitive to symmetry energy and is insensitive to the isospin dependence of nn cross section. The decrease in  $E_{bal}$  with increase in  $N/Z$  ratio is due to the enhanced role of repulsive symmetry energy for higher  $N/Z$  ratios. To check the role of symmetry energy on the  $N/Z$  dependence of  $E_{bal}$ , in Ref. [12] Gautam and Sood reduces the strength of potential part of symmetry energy to zero and calculate the  $E_{bal}$ . So here also to see the effect of symmetry energy, we reduce its strength to zero and calculate  $E_{bal}$  for two extreme systems of Ca+Ca and Xe+Xe series. The results are displayed in Fig. 2 (open symbols). Top, middle and bottom panels represent the results for  $b/b_{max} = 0.2-0.4$ ,  $0.4-0.6$  and  $0.6-0.8$ , respectively. From figure we see that  $E_{bal}$  increases for both the masses on reducing the strength of symmetry potential whereas the slope of  $N/Z$  dependence of  $E_{bal}$  decreases drastically for both the systems. From figure, we also see that percentage change ( $\Delta m(\%) = \frac{m - m_{symmoff}}{m}$ ) in slope for Ca (Xe) series is 67 (93) at  $b/b_{max} = 0.2-0.4$  whereas it is 64 (89) at  $b/b_{max} = 0.4-0.6$ .

In fig. 3, we display the percentage difference of  $E_{bal}$  ( $\Delta E_{bal}(\%) = \frac{E_{bal}^{symmoff} - E_{bal}}{E_{bal}} * 100$ ) between calculations without symmetry energy and with symmetry energy as a function of  $N/Z$  for at  $b/b_{max} = 0.2-0.4$  (top panel),  $0.4-0.6$  (middle panel) and  $0.6-0.8$  (bottom panel). From fig. we find that

- (i) the percentage difference increases with  $N/Z$  for both the system masses at all the

colliding geometries indicating that the role of symmetry energy increases with  $N/Z$  ratio (ii) and the increase is more sharp for Ca series as compared to Xe series at semicentral and semiperipheral collisions whereas at peripheral collisions, the increase is almost the same for both the masses.

(iii) Also, for a particular mass,  $\Delta E_{bal}(\%)$  rises with impact parameter and increase with impact parameter is more for Xe series as compared to the Ca series.

In figs. 4 and fig. 5 we display the system size dependence of  $E_{bal}$  for various  $N/Z$  ratios varying from 1.0 to 2.0 for  $b/b_{max} = 0.4 - 0.6$  and  $b/b_{max} = 0.6 - 0.8$ , respectively. The results are displayed by open squares, triangles, circles, diamonds, pentagons, and left triangles, for  $N/Z$  ratios of 1.0, 1.2, 1.4, 1.6, 1.8, and 2.0, respectively. From fig. 4, we see that  $E_{bal}$  follows a power law behavior ( $\propto A^\tau$ ) with system size. The power law parameter  $\tau$  is  $-0.50 \pm 0.02$ ,  $-0.46 \pm 0.02$ ,  $-0.41 \pm 0.02$ ,  $-0.34 \pm 0.03$ ,  $-0.33 \pm 0.03$ , and  $-0.22 \pm 0.03$ , respectively, for  $N/Z$  ratios of 1.0, 1.2, 1.4, 1.6, 1.8, and 2.0. We find that the power law parameter goes on decreasing as we are moving towards asymmetric nuclear matter (higher  $N/Z$ ). This is due to the fact that for higher  $N/Z$  ratios, the effect of symmetry energy is more in lighter masses (as in Ref. [12]) and thus decreasing  $E_{bal}$  by larger magnitude in lighter masses which results in less slope for higher  $N/Z$  ratio.

Fig. 5 displays the system size effect of  $E_{bal}$  at peripheral colliding geometry of  $b/b_{max} = 0.6 - 0.8$ . The behavior of  $E_{bal}$  with system size is similar, except that now the value of power law parameter is increased. The value of  $\tau$  now reads as  $-1.03 \pm 0.01$ ,  $-0.87 \pm 0.03$ ,  $-0.81 \pm 0.02$ ,  $-0.72 \pm 0.02$ ,  $-0.63 \pm 0.03$ , and  $-0.59 \pm 0.03$ , respectively, for  $N/Z$  ratios of 1.0, 1.2, 1.4, 1.6, 1.8, and 2.0. The increase in the value of slope parameter is due to the fact that  $E_{bal}$  for lighter systems (like Ca+Ca) changes drastically with impact parameter but the change of  $E_{bal}$  with impact parameter in heavier masses is less [23] which leads in the increase of slope parameter at peripheral colliding geometries.

In Fig. 6 we show  $N/Z$  dependence of  $\tau$  for the impact parameter bins of  $b/b_{max} = 0.2 - 0.4$  (black hexagons) ( $\tau$  values taken from Ref. [11]),  $b/b_{max} = 0.4 - 0.6$  (green hexagons) and  $b/b_{max} = 0.6 - 0.8$  (orange hexagons). We see that  $\tau$  decreases with increase in  $N/Z$  ratio for all the colliding geometries and follows a linear behavior with  $N/Z$  having slopes 0.13, 0.27, and 0.43 for  $b/b_{max} = 0.2 - 0.4$ ,  $0.4 - 0.6$ , and  $0.6 - 0.8$ , respectively. We also find that change in slope is more when we move from semi peripheral to peripheral geometry as compared to that when we move from semi central to semi peripheral collisions.

## 4 Summary

We have studied the role of colliding geometry on N/Z dependence of balance energy ( $E_{bal}$ ) for isotopic series throughout the mass range. We found that dependence of  $E_{bal}$  on N/Z ratio is much stronger for peripheral collisions as compared to the central collisions. Our study also pointed out that lighter systems showed more sensitivity to the colliding geometry towards N/Z dependence of  $E_{bal}$ . We have also studied the mass dependence of  $E_{bal}$  for the N/Z range from 1.0-2.0 for the whole range of colliding geometry. We found that the mass dependence of  $E_{bal}$  varies with the N/Z ratio.

This work is supported by a grant from Centre of Scientific and Industrial Research (CSIR), Government of India and Indo-French center vide project no-4101-A, New Delhi, India.

## References

- [1] W. Zhan *et al.*, Int. J. Mod. Phys. E **15**, 1941 (2006); see, e.g. <http://www.impcas.ac.cn/zhuye/en/htm/247.htm>.
- [2] See, e.g., [http://www.gsi.de/fair/index\\_e.html](http://www.gsi.de/fair/index_e.html); See, e.g., <http://ganiinfo.in2p3.fr.research/developments/spiral2>.
- [3] Y. Yano, Nucl. Inst. Methods B **261**, 1009 (2007).
- [4] B. A. Li, Z. Ren, C. M. Ko, and S. J. Yennello, Phys. Rev. Lett. **76**, 4492 (1996); C. Liewen, Z. Fengshou, and J. Genming, Phys. Rev. C **58**, 2283 (1998); L. Scalone, M. Colonna and M Di Toro, Phys. Lett. B **461**, 9 (1999).
- [5] R. Pak *et al.*, Phys. Rev. Lett. **78**, 1022 (1997); *ibid.* **78**, 1026 (1997).
- [6] S. Gautam *et al.*, J. Phys. G: Nucl. Part. Phys. **36**, 085102 (2010).
- [7] D. Q. Fang *et al.*, Phys. Rev. C **64**, 044610 (2000); G. J. Kunde *et al.*, Phys. Rev. Lett. **77**, 2897 (1996); F. S. Zhang *et al.*, Phys. Rev. C **60**, 064604 (1999).
- [8] M. C. Wang *et al.*, Phys. Rev. C **79**, 034606 (2009); M. B. Tsang *et al.*, Phys. Rev. Lett. **92**, 062701 (2004); Z. Kohley *et al.*, Phys. Rev. C **83**, 044601 (2011).
- [9] S. Gautam and A. D. Sood, Phys. Rev. C **82**, 014604 (2010).

- [10] S. Gautam, A. D. Sood, R. K. Puri, and J. Aichelin, Phys. Rev. C, **83**, 014603 (2011).
- [11] A. D. Sood, Phys. Rev. C, in press (2011).
- [12] S. Gautam and A. D. Sood, Phys. Rev. C, communicated (2011).
- [13] C. Hartnack *et al.*, Eur. Phys. J. A **1**, 151 (1998); C. Hartnack and J. Aichelin, Phys. Rev. C **49**, 2801 (1994); S. Kumar *et al.*, *ibid.* **81**, 014611 (2010); *ibid.* **81**, 014601 (2010).
- [14] J. Aichelin, Phys. Rep. **202**, 233 (1991); E. Lehmann, R. K. Puri, A. Faessler, G. Batko, and S. W. Huang, Phys. Rev. C **51**, 2113 (1995); Y. K. Vermani *et al.*, J. Phys. G: Nucl. Part. Phys. **36**, 105103 (2009); *ibid.* **37**, 115105 (2010); *ibid.* Eur Phys Lett **85**, 62001 (2010); *ibid.* Phys. Rev. C **79**, 064613 (2009), Nucl. Phys A **847**, 243 (2010).
- [15] H. Kruse, B. V. Jacak and H. Stöcker, Phys. Rev. Lett. **54**, 289 (1985); J. J. Molitoris and H. Stöcker, Phys. Rev. C **32**, 346 (R) (1985).
- [16] J. Cugnon, T. Mizutani, and J. Vandermeulen, Nucl. Phys. **A352**, 505 (1981).
- [17] A. D. Sood and R. K. Puri, Phys. Rev. C **69**, 054612 (2004).
- [18] A. D. Sood and R. K. Puri, Phys. Lett. **B594**, 260 (2004).
- [19] G. D. Westfall *et al.*, Phys. Rev. Lett. **71**, 1986 (1993).
- [20] G. D. Westfall, Nucl. Phys. **A630**, 27c (1998).
- [21] D. Cussol *et al.*, Phys. Rev. C **65**, 044604 (2002).
- [22] C. A. Ogilvie *et al.*, Phys. Rev. C **40**, 2592 (1989).
- [23] D. J. Magestro, W. Bauer, and G. D. Westfall, Phys. Rev. C **62**, 041603(R) (2000); R. Chugh and R. K. Puri, Phys. Rev. C **82**, 014603 (2010); D. Klakow, G. Welke, and W. Bauer, Phys. Rev. C **48**, 1982 (1993).



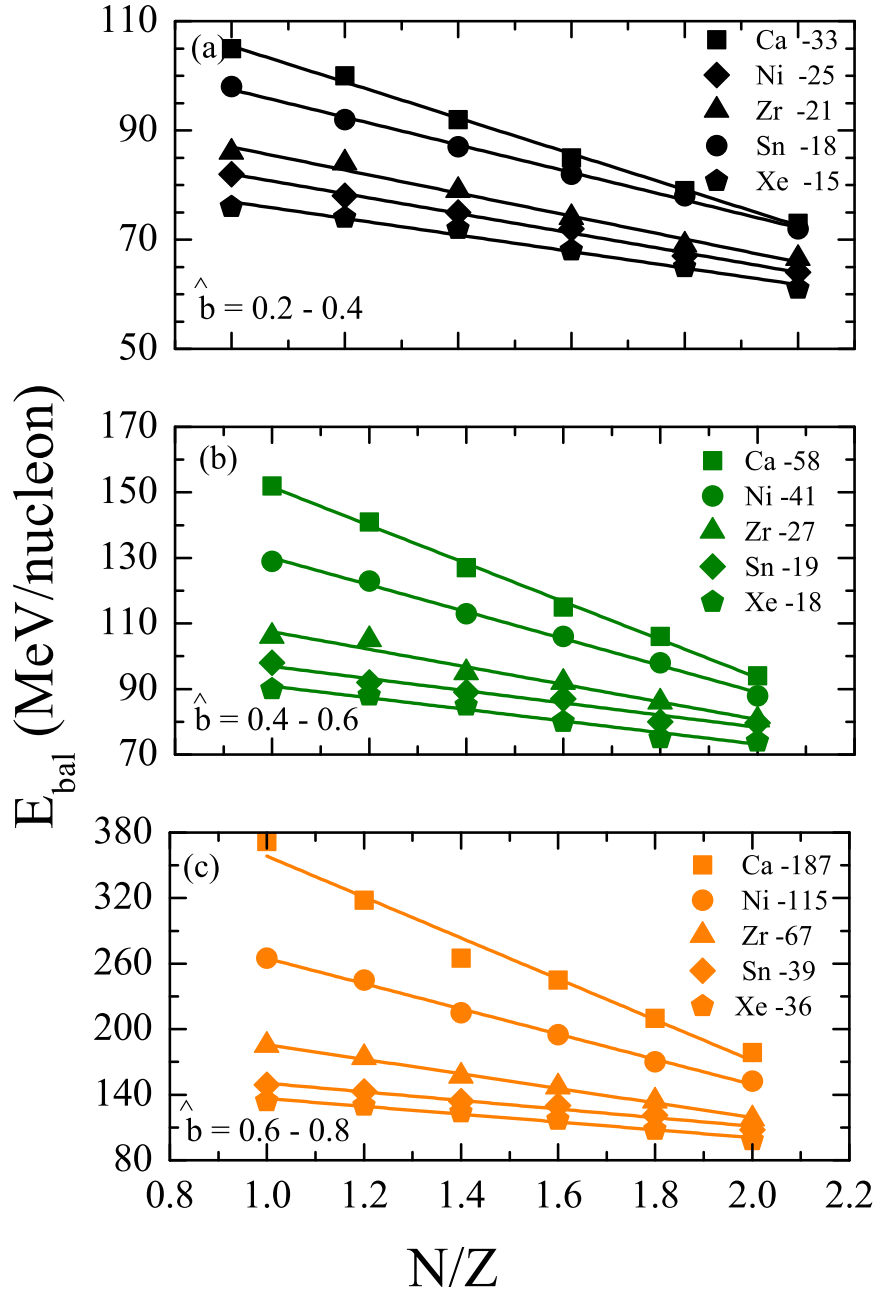


Figure 1: N/Z dependence of  $E_{bal}$  for various systems. Various symbols are explained in the text. Lines are linear fit. Top, middle and bottom panels represent the results for  $b/b_{max} = 0.2 - 0.4$ ,  $0.4 - 0.6$  and  $0.6 - 0.8$ , respectively.

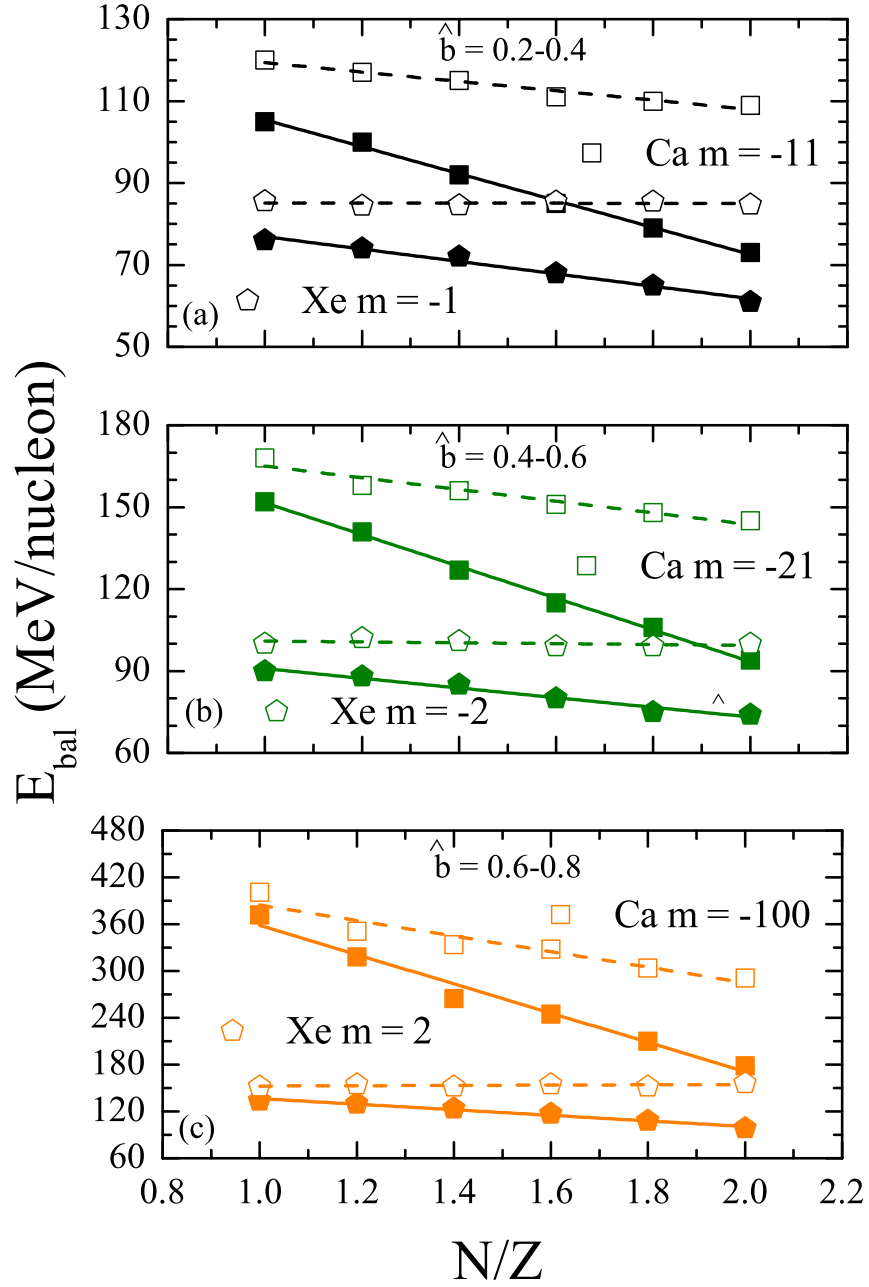


Figure 2: N/Z dependence of  $E_{bal}$  for Ca+Ca and Xe+Xe with  $E_{sym}$  on and off. Various symbols are explained in text. Top, middle and bottom panels represent the results for  $b/b_{max} = 0.2 - 0.4$ ,  $0.4 - 0.6$  and  $0.6 - 0.8$ , respectively.

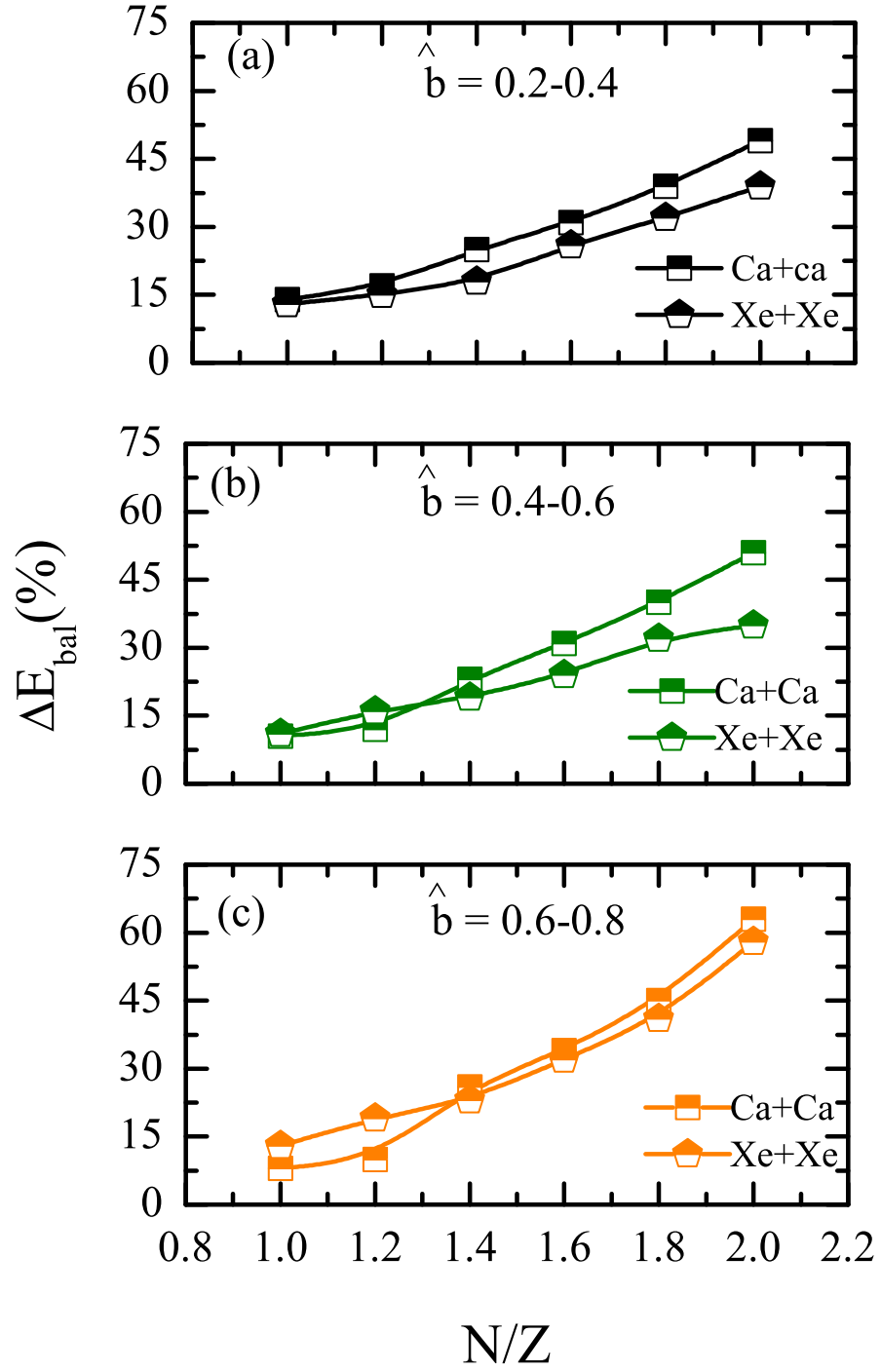


Figure 3:  $N/Z$  dependence of  $\Delta E_{bal}(\%)$  for Ca and Xe series. Various symbols are explained in text. Lines are guide to the eye. 11

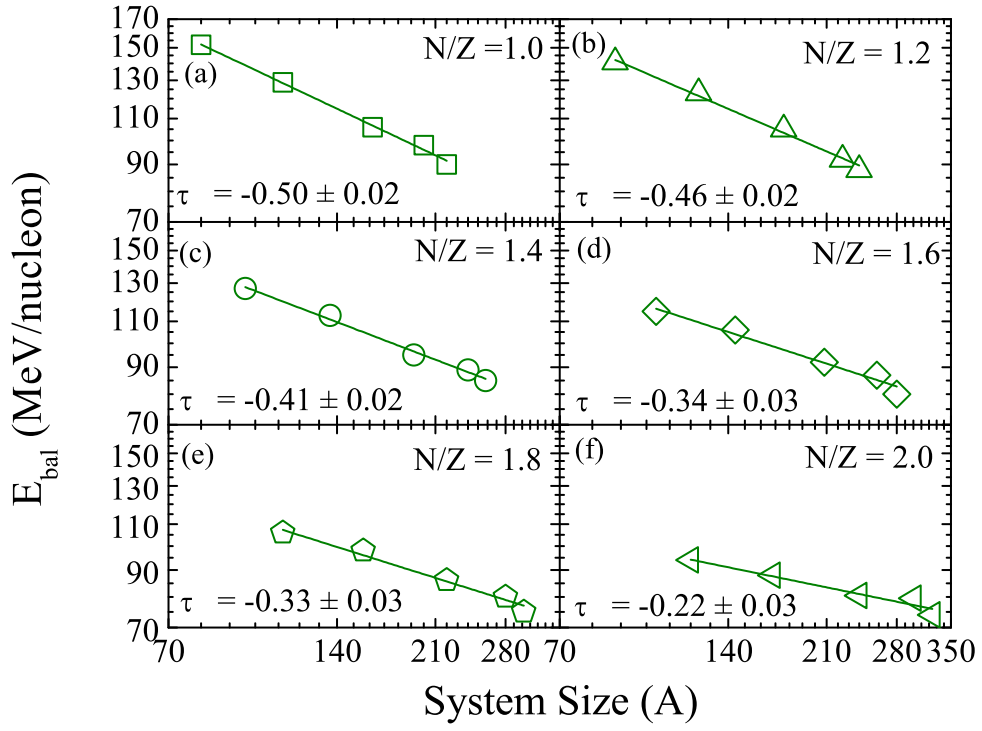


Figure 4: System size dependence of  $E_{bal}$  for various  $N/Z$  ratios at  $b/b_{max} = 0.4-0.6$ . Lines are of power law nature ( $\propto A^\tau$ ).

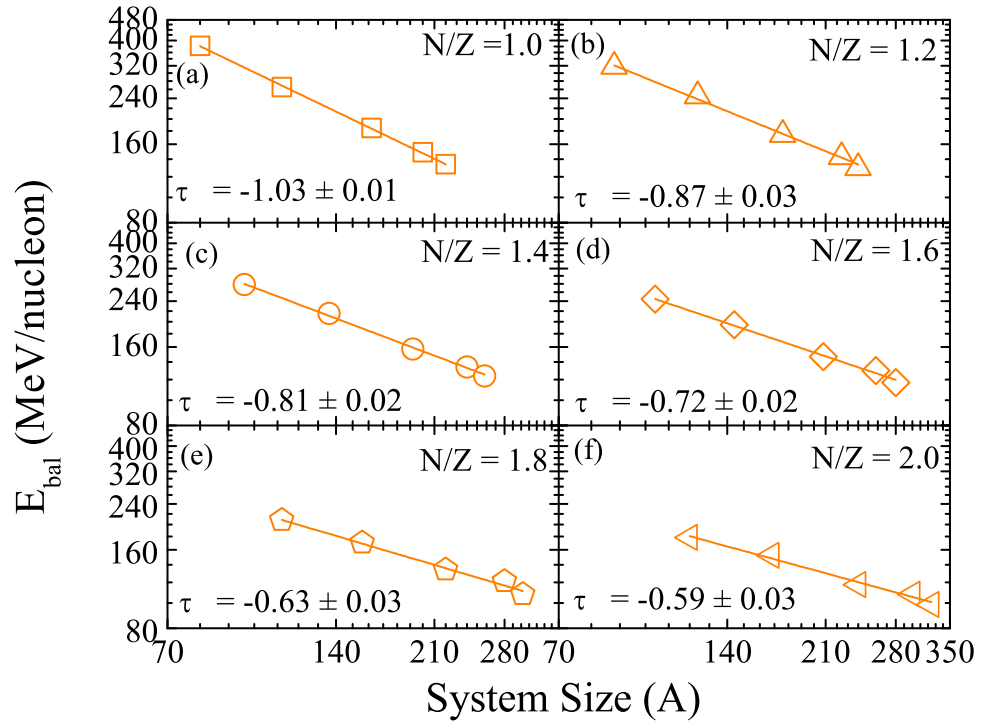


Figure 5: Same as fig. 4 but for  $b/b_{\text{max}} = 0.6-0.8$ .

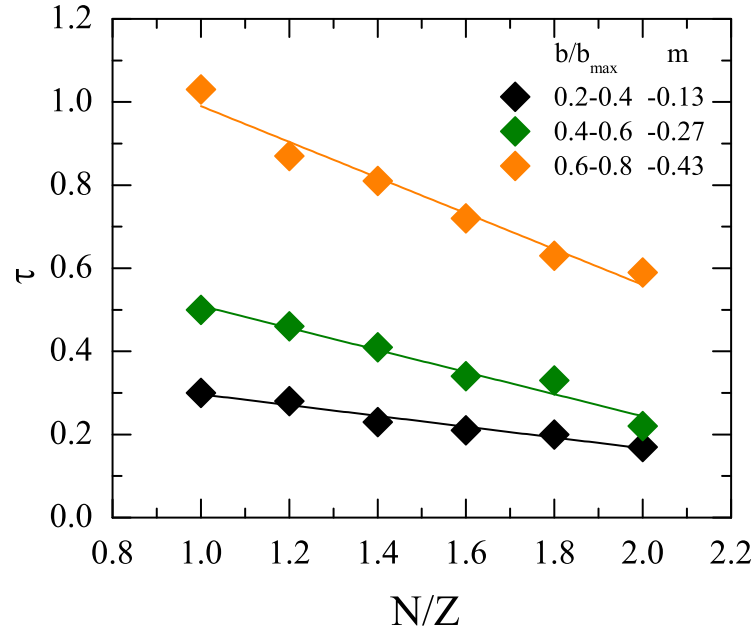


Figure 6:  $N/Z$  dependence of  $\tau$ . Lines are of linear fit.